WASP-35b, WASP-48b, AND HAT-P-30b/WASP-51b: TWO NEW PLANETS AND AN INDEPENDENT DISCOVERY OF A HAT PLANET

B. Enoch[1], D. R. Anderson[2], S. C. C. Barros[3], D. J. A. Brown[1], A. Collier Cameron[1], F. Faedi[3], M. Gillon[4],
G. Hébrard[5,6], T. A. Lister[7], D. Queloz[8], A. Santerne[9], B. Smalley[2], R. A. Street[7], A. H. M. J. Triaud[8], R. G. West[10],
F. Bouchy[5,6], J. Bento[11], O. Butters[10], L. Fossati[12], C. A. Haswell[12], C. Hellier[2], S. Holmes[12], E. Jehen[4], M. Lendl[8],
P. F. L. Maxted[2], J. McCormac[3], G. R. M. Miller[1], V. Moulds[3], C. Moutou[9], A. J. Norton[12], N. Parley[1], F. Pepe[8],
D. Pollacco[3], D. Segransan[8], E. Simpson[3], I. Skillen[13], A. M. S. Smith[2], S. Udry[8], AND P. J. Wheatley[11]

[1] SUPA, School of Physics and Astronomy, University of St Andrews, North Haugh, St Andrews KY16 9SS, UK
[2] Astrophysics Group, Keele University, Staffordshire ST5 5BG, UK
[3] Astrophysics Research Centre, School of Mathematics & Physics, Queen's University Belfast, University Road, Belfast BT7 1NN, UK
[4] Institut d'Astrophysique et de Géophysique, Université de Liége, Allée de 6 Août, 17, Bat B5C, Liége 1, Belgium
[5] Institut d'Astrophysique de Paris, UMR7095 CNRS, Université Pierre & Marie Curie, France
[6] Observatoire de Haute-Provence, CNRS/OAMP, 04870 St Michel l'Observatoire, France
[7] Las Cumbres Observatory, 6740 Cortona Drive Suite 102, Goleta, CA 93117, USA
[8] Observatoire Astronomique de l'Université de Genéve, 51 Chemin des Maillettes, 1290 Sauverny, Switzerland
[9] Laboratoire d'Astrophysique de Marseille, Université d'Aix-Marseille & CNRS, 38 rue Frédéric Joliot-Curie, 13388 Marseille Cedex 13, France
[10] Department of Physics and Astronomy, University of Leicester, Leicester LE1 7RH, UK
[11] Department of Physics, University of Warwick, Coventry CV4 7AL, UK
[12] Department of Physics and Astronomy, The Open University, Milton Keynes MK7 6AA, UK
[13] Isaac Newton Group of Telescopes, Apartado de Correos 321, E-38700 Santa Cruz de Palma, Spain

ABSTRACT

We report the detection of WASP-35b, a planet transiting a metal-poor ([Fe/H] $= -0.15$) star in the Southern hemisphere, WASP-48b, an inflated planet which may have spun-up its slightly evolved host star of 1.75 $R_\odot$ in the Northern hemisphere, and the independent discovery of HAT-P-30b/WASP-51b, a new planet in the Northern hemisphere. Using WASP, RISE, Faulkes Telescope South, and TRAPPIST photometry, with CORALIE, SOPHIE, and NOT spectroscopy, we determine that WASP-35b has a mass of $0.72 \pm 0.06\,M_J$ and radius of $1.32 \pm 0.05\,R_J$, and orbits with a period of 3.16 days, WASP-48b has a mass of $0.98 \pm 0.09\,M_J$, radius of $1.67 \pm 0.10\,R_J$, and orbits in 2.14 days, while HAT-P-30b/WASP-51b, with an orbital period of 2.81 days, is found to have a mass of $0.76 \pm 0.05\,M_J$ and radius of $1.42 \pm 0.03\,R_J$, agreeing with values of $0.71 \pm 0.03\,M_J$ and $1.34 \pm 0.07\,R_J$ reported for HAT-P-30b.

Key words: planetary systems

Online-only material: color figures

1. INTRODUCTION

Around 120 transiting exoplanets have now been discovered,[14] having both their radii and masses known, and may be subjected to further investigations into their bulk and atmospheric composition (see, e.g., Charbonneau et al. 2002, 2005; Fortney et al. 2007; Haswell 2010; Seager & Deming 2010). They show a diverse range of densities and thus internal compositions. Over 80% of those with masses greater than $0.1\,M_J$ have radii greater than that of Jupiter, and many have extremely low densities which even coreless models struggle to explain (Fortney et al. 2007; Burrows et al. 2007), for example TrES-4b (Mandushev et al. 2007), WASP-17b (Anderson et al. 2010, 2011), and Kepler-7b (Latham et al. 2010). More transiting exoplanets are vital to constrain the formation and evolution of such planets.

Several possible effects on planetary radii have been discussed in the literature, including inflation due to strong heating by irradiation received from the host star (Guillot et al. 1996; Guillot & Showman 2002), ohmic heating from the coupling of magnetic fields and atmospheric flows (Batygin & Stevenson 2010; Batygin et al. 2011), and tidal heating due to the circularization of close-in exoplanets (Bodenheimer et al. 2001, 2003; Jackson et al. 2008).

Most of the known transiting exoplanets orbit very close to their host star, which produces strong tidal forces between them. The tidal interactions may result in orbital circularization, synchronization, and decay (Pont 2009). An apparent relationship between period and eccentricity of non-transiting exoplanets, such that planets very close to their host stars have circular orbits while those farther from the stars show a wide range of eccentricities, seems to provide evidence for the tidal circularization of planetary orbits (Mazeh 2008). However, it had generally been assumed that the masses of planets are too small to synchronize the stellar rotation with the planetary orbit through tidal forces (Mazeh 2008). Some possible exceptions exist for planets with large masses, for example the τ Boo system with a $4\,M_J$ planet, for which there is evidence for stellar rotation synchronization (Fares et al. 2009). Recently, CoRoT-11b has been announced to have a "peculiar tidal evolution" (Gandolfi et al. 2011), where the stellar rotation period of 1.7 days is now shorter than the planetary orbital period of 3 days, due to the strong tidal forces causing orbital expansion of the planet from a previously approximately synchronized orbital period. The possibility of perhaps unknown close-in exoplanets affecting the stellar spin rate of their host stars produces uncertainty in the use of the gyrochronological age estimate of a star, based on the normal spin-down of a star as it ages.

---

[14] http://www.exoplanet.eu.

Table 1
Star Locations

Star	R.A. (J2000)	Decl. (J2000)	V mag (Tycho-2[a])
WASP-35	05 04 19.6	−06 13 47	11.01 ± 0.09
WASP-48	19 24 39.0	+55 28 23	11.72 ± 0.14
HAT-P-30/WASP-51	08 15 48.0	+05 50 12	10.42 ± 0.05

Note. [a] Høg et al. (2000).

One motivation of the Wide Angle Search for Planets (WASP) project is to discover enough transiting exoplanets with a wide range of orbital and compositional parameters to allow analyses that may distinguish between different models. Recent WASP discoveries help fill in areas of planetary mass–radius parameter space, for example, WASP-39b (Faedi et al. 2011) is the least dense sub-Saturn-mass planet known.

Here, we announce WASP-35b and WASP-48b and describe the independent discovery of HAT-P-30b, designated WASP-51b by us: the positions and magnitudes of each star are given in Table 1. We set out the photometric and spectroscopic observations obtained for each system, before presenting the resulting stellar and system parameters. WASP-48 appears to be a slightly evolved star with a large radius of 1.75 $R_\odot$ and a very short rotation period of around 7 days for its age, around 8 Gyr. WASP-48b may therefore have spun-up its host star despite a mass of only around 1 M_J, due to the star's inflated radius, although the system has not yet reached synchronization of stellar rotation period with planetary orbital period (2.15 days). As the host star continues to evolve, increasing significantly in radius, it may engulf WASP-48b, which is currently orbiting at a distance of around four times the stellar radius, unless orbital expansion due to tidal interactions, such as may have happened to CoRoT-11b (Gandolfi et al. 2011), pushes the planet far enough away to survive.

2. OBSERVATIONS

2.1. Photometric Observations

The WASP-North and South observatories are located at La Palma, Canary Islands, and SAAO, South Africa, respectively, and each consist of eight 11 cm telescopes of $7^\circ.8 \times 7^\circ.8$ field of view each, on a single fork mount. The cameras scan repeatedly through eight to ten sets of fields each night, taking 30 s exposures. See Pollacco et al. (2006) for more details on the WASP project and the data reduction procedure, and Collier Cameron et al. (2007) and Pollacco et al. (2008) for an explanation of the candidate selection process.

High-precision transit light curves of WASP-35, WASP-48, and HAT-P-30/WASP-51 were obtained with the Rapid Imager to Search for Exoplanets (RISE) instrument mounted in the 2.0 m Liverpool Telescope (Steele et al. 2008; Gibson et al. 2008) at the Observatorio del Roque de los Muchachos on La Palma, Canary Islands. The data were reduced with the ULTRACAM pipeline (Dhillon et al. 2007) following the same procedure as Barros et al. (2011). Further high-quality photometry of WASP-35 was obtained with the 0.6 m TRAnsiting Planets and PlanetesImals Small Telescope (TRAPPIST) at La Silla Observatory, Chile, and with the LCOGT 2.0 m Faulkes Telescope South (FTS) at Siding Spring Observatory.

Photometric observations for each of WASP-35, WASP-48, and HAT-P-30/WASP-51 are detailed in Table 2 and shown in Figures 1–3.

Table 2
Photometric Observations

Instrument	Date(s)	No. of Data Points
	WASP-35	
WASP-N (2 cams)	2008 Oct–2009 Jan	16,748
	2009 Oct–2010 Jan	
WASP-S (1 cam)	2009 Oct–2010 Jan	
RISE ($V + R$)	2010 Nov 30	630
TRAPPIST ($I + z$)	2010 Dec 23	742
FTS (z)	2011 Jan 1	205
TRAPPIST ($I + z$)	2011 Jan 11	300
	WASP-48	
WASP-N (3 cams)	2007 May–2007 Jul	56,036
	2008 May–2008 Aug	
	2009 May–2009 Jun	
	2010 May–2010 Sep	
RISE ($V + R$)	2010 Jul 1	770
	HAT-P-30/WASP-51	
WASP-N (1 cam)	2009 Nov–2010 Mar	4453
RISE ($V + R$)	2011 Jan 12	1245

2.2. Spectroscopic Observations

We obtained three radial velocity (RV) measurements of WASP-35 on 2010 January 25 and 26 with the FIbre-fed Echelle Spectrograph (FIES) on the 2.5 m Nordic Optical Telescope (NOT).[15] FIES was used in medium resolution mode ($R = 46,000$) with simultaneous ThAr calibration, and the observations were reduced using the FIEStool package,[16] then cross-correlated with a high signal-to-noise spectrum of the Sun to obtain the radial velocities. A further nine data points were obtained with the CORALIE echelle spectrograph mounted on the Swiss telescope at the ESO La Silla Observatory in Chile on 2010 January 5 and between 2010 February 6 and 14 and the resulting spectra were processed with the standard data reduction CORALIE pipeline (Baranne et al. 1996; Mayor et al. 2009), plus a correction for the blaze function (Triaud 2010).

WASP-48 was observed spectroscopically with the SOPHIE fiber-fed echelle spectrograph mounted on the 1.93 m telescope at Observatoire de Haute-Provence (OHP) (Perruchot et al. 2008; Bouchy et al. 2009). Fourteen data points were taken in high efficiency mode ($R = 40,000$) between 2010 April 19 and October 18, obtaining a signal-to-noise ratio (S/N) of around 35 for each. Wavelength calibration with a thorium–argon lamp was performed to allow the interpolation of the spectral drift of SOPHIE.

Radial velocity observations of HAT-P-30/WASP-51 were made with the CORALIE and SOPHIE spectrographs. Nine data points were taken with SOPHIE between 2010 October 16 and November 25, using the high-resolution mode ($R = 75,000$) and obtaining an S/N of around 20 for each measurement. Ten further data points were obtained with CORALIE between 2010 December 7 and 2011 January 4.

The radial velocities measured using these spectra are given in Tables 3–5 and shown as a function of orbital phase in Figures 4–6, along with radial velocity residuals and bisector span variations. The radial velocity measurements show low-amplitude variations, compatible with the existence of orbiting

---

[15] Operated on the island of La Palma jointly by Denmark, Finland, Iceland, Norway, and Sweden, in the Spanish Observatorio del Roque de los Muchachos of the Instituto de Astrofisica de Canarias.
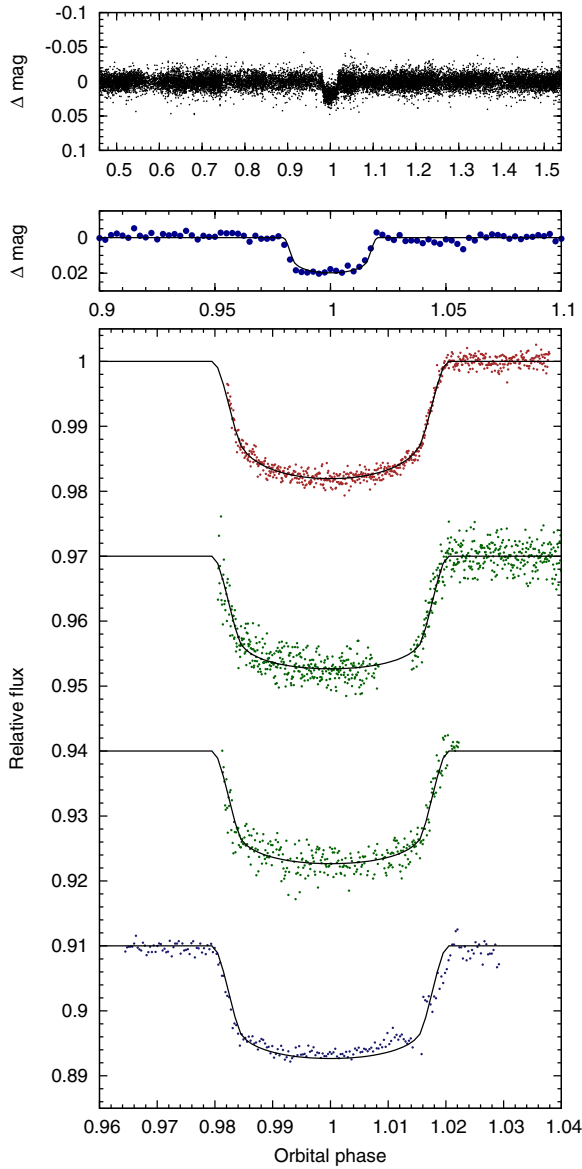[16] http://www.not.iac.es/instruments/fies/fiestool/FIEStool.html.

Figure 1. Top: WASP-35 discovery light curve folded on the orbital period of $P = 3.16$ days. Middle: WASP data binned in phase, with bin width = 11 minutes. Bottom (top to bottom): transit obtained with the RISE instrument on 2010 November 30, TRAPPIST on 2010 December 23 and 2011 January 11, and FTS on 2011 January 1; light curves offset for clarity.

(A color version of this figure is available in the online journal.)

Table 3
Radial Velocity Measurements of WASP-35

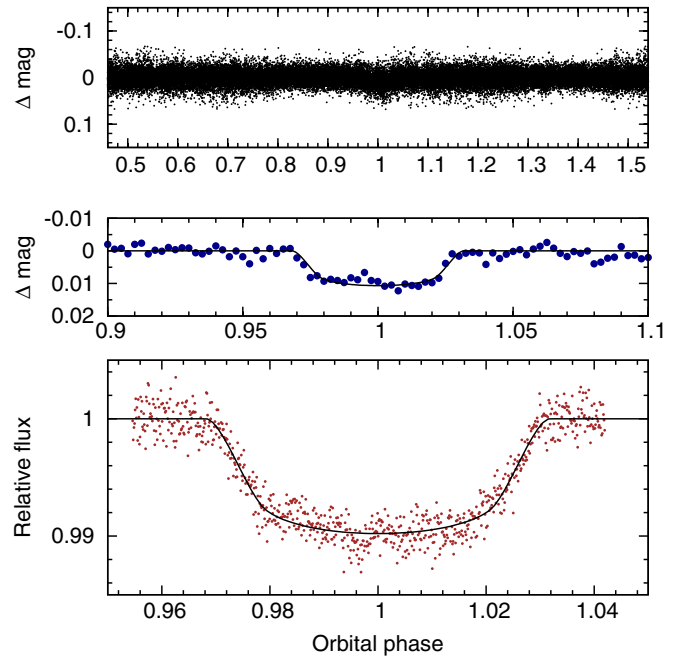| BJD–2 400 000	RV (km s^{-1})	σ_{RV} (km s^{-1})	BS (km s^{-1})	Instrument
5201.7298	17.8174	0.0085	−0.0225	CORALIE
5221.5256	17.7386	0.0096		FIES
5222.3276	17.6211	0.0079		FIES
5222.5131	17.6318	0.0093		FIES
5233.6480	17.8050	0.0133	−0.0020	CORALIE
5235.6597	17.6897	0.0084	−0.0446	CORALIE
5236.5322	17.8342	0.0078	−0.0531	CORALIE
5237.5430	17.7133	0.0081	−0.0172	CORALIE
5238.5912	17.6439	0.0080	0.0069	CORALIE
5239.6245	17.8183	0.0088	−0.0402	CORALIE
5240.5331	17.7754	0.0128	−0.0087	CORALIE
5241.5318	17.6446	0.0075	−0.0201	CORALIE

Figure 2. Top: WASP-48 discovery light curve folded on the orbital period of $P = 2.14$ days. Middle: WASP data binned in phase, with bin width = 8 minutes. Bottom: transit obtained with the RISE instrument on 2010 July 1.

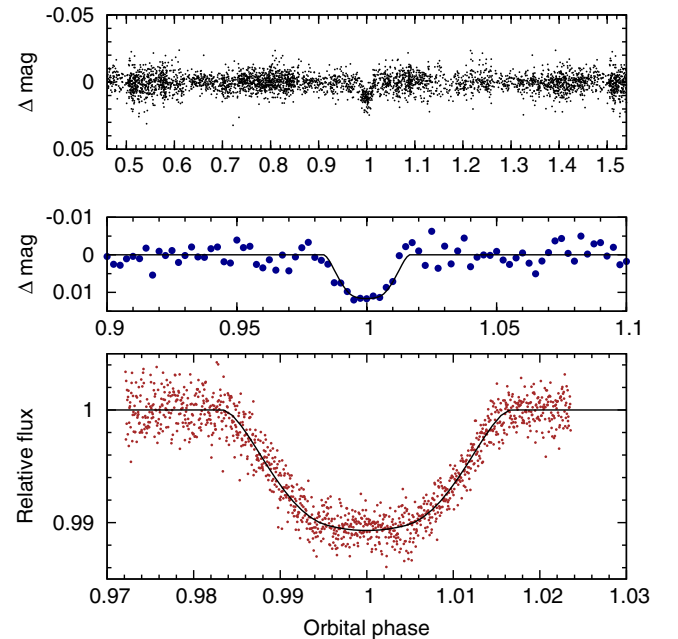(A color version of this figure is available in the online journal.)

Figure 3. Top: HAT-P-30/WASP-51 discovery light curve folded on the orbital period of $P = 2.81$ days. Middle: WASP data binned in phase, with bin width = 10 minutes. Bottom: transit obtained with the RISE instrument on 2011 January 12.

(A color version of this figure is available in the online journal.)

planets, and are not correlated with the bisector spans (Queloz et al. 2001), available for CORALIE and SOPHIE data (no correlation is found with p-value less than 0.05), which could indicate stellar blend configurations.

The CORALIE guiding camera revealed a faint star located at about 1″5 from HAT-P-30/WASP-51 which was observed simultaneously with HAT-P-30/WASP-51 through the 3″ fiber of the SOPHIE spectrograph. This target was too close and

Table 4
Radial Velocity Measurements of WASP-48 Taken with the
SOPHIE Spectrograph

BJD-2 400 000	RV (km s^{-1})	$\sigma_{\rm RV}$ (km s^{-1})	BS (km s^{-1})
5305.6441	−19.711	0.024	−0.029
5323.5842	−19.648	0.021	0.015
5328.5784	−19.831	0.025	−0.083
5409.4890	−19.667	0.026	−0.071
5427.5503	−19.747	0.023	−0.062
5429.4215	−19.809	0.026	−0.044
5431.4254	−19.831	0.033	−0.014
5432.3967	−19.589	0.036	−0.059
5476.2714	−19.745	0.021	−0.002
5477.2679	−19.591	0.026	0.044
5482.2945	−19.594	0.022	−0.029
5484.2801	−19.529	0.020	0.042
5485.2880	−19.823	0.026	−0.027
5488.2831	−19.569	0.036	0.009

Table 5
Radial Velocity Measurements of HAT-P-30/WASP-51

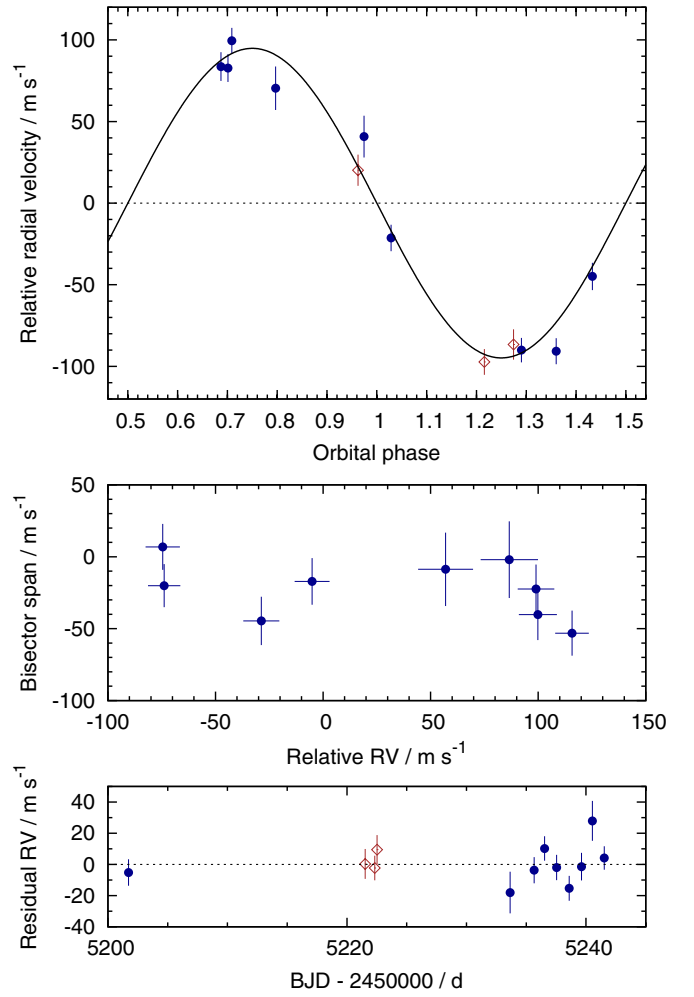| BJD-2 400 000	RV (km s^{-1})	$\sigma_{\rm RV}$ (km s^{-1})	BS (km s^{-1})	Instrument
5485.6249	44.611	0.018	−0.023	SOPHIE
5489.6119	44.783	0.018	−0.017	SOPHIE
5495.6696	44.708	0.015	0.100	SOPHIE
5513.6757	44.596	0.013	−0.013	SOPHIE
5519.6870	44.657	0.014	−0.002	SOPHIE
5522.6691	44.677	0.015	0.038	SOPHIE
5523.7176	44.754	0.023	0.084	SOPHIE
5524.6337	44.593	0.022	−0.055	SOPHIE
5525.6785	44.771	0.021	−0.003	SOPHIE
5527.6506	44.586	0.015	0.048	SOPHIE
5537.8023	44.7111	0.0062	−0.0046	CORALIE
5538.8006	44.5639	0.0061	−0.0118	CORALIE
5542.8449	44.7469	0.0073	0.0240	CORALIE
5544.7669	44.6278	0.0065	0.0087	CORALIE
5545.8487	44.7761	0.0066	0.0016	CORALIE
5547.8576	44.6832	0.0074	−0.0027	CORALIE
5561.8052	44.6526	0.0072	0.0241	CORALIE
5562.8426	44.7309	0.0070	−0.0010	CORALIE
5563.7958	44.5945	0.0083	0.0155	CORALIE
5565.7984	44.7353	0.0070	0.0170	CORALIE

Figure 4. Radial velocity measurements for WASP-35: red, open diamonds denote NOT observations, blue circles are from CORALIE. The solid line shown on the top plot is the best-fitting MCMC solution with eccentricity fixed to zero. The center-of-mass velocity, $\gamma = 17.71$ km s^{-1}, was subtracted. The middle plot shows the bisector span variations against radial velocity measurements. The uncertainty in the bisector span measurements is taken to be twice the uncertainty in the radial velocity measurements. The bottom plot shows the radial velocity residuals against time.

(A color version of this figure is available in the online journal.)

too faint to perform aperture photometry with the CORALIE guiding images in order to estimate the magnitude. Thus, we performed radial velocity blend simulations (A. Santerne et al. 2011, in preparation) in order to investigate whether small bisector variations seen in SOPHIE data are due to this secondary blending star, though the bisector spans are compatible with no variation within the 2σ level. This simulation consisted of producing SOPHIE cross-correlation functions (CCFs) for HAT-P-30/WASP-51 with the unblended orbital solution seen by CORALIE and blending a single (solar) star with different systemic radial velocity, distance ratio from HAT-P-30/WASP-51, and $v \sin i$. Since the distance between the two stars is degenerate with their surface brightness different, and without any magnitude constraint on the second star, we assumed it to be a solar-type star in order to simplify the simulation. We carry out 10,000 Monte Carlo simulations with the following input parameters: the systemic RV was chosen in a range 34.6–54.6 km s^{-1} since the two stars have to be well aligned in velocity to reproduce such a symmetric bisector

effect, the distance ratio of HAT-P-30/WASP-51 was chosen between 1 and 5 (a solar star five times further from HAT-P-30/WASP-51 is too faint to significantly affect its CCF), and finally we test the $v \sin i$ of the blending star between 4 and 40 km s^{-1}. We did not find any significant model that reproduces the bisector effect seen in the SOPHIE data with the observed bisector amplitude. To reproduce such a bisector span, it is necessary to have much larger semi-amplitude RV variations coupled with an RV-aligned blend which is not compatible with the CORALIE nor HIRES (Johnson et al. 2011) data. In the case of HAT-P-30/WASP-51, the effect of the blending star on the bisector is at a level of a few m s^{-1}. We concluded that the faint star 1″5 away did not significantly affect the SOPHIE CCF of HAT-P-30/WASP-51.

3. RESULTS AND DISCUSSION

3.1. Stellar Parameters

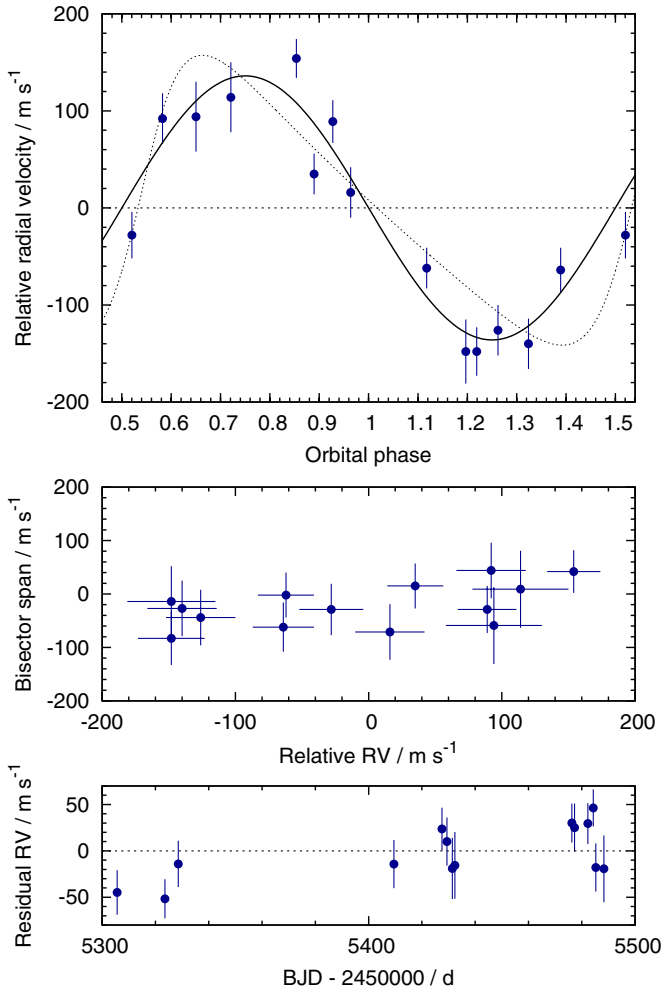The individual NOT/FIES spectra of WASP-35 were co-added to produce a single spectrum with an average S/N of

Figure 5. Radial velocity measurements for WASP-48: details are as for WASP-35, with center-of-mass velocity, $\gamma = -19.68$ km s^{-1} here. An eccentric solution resulting from modeling the system with an enforced main-sequence constraint and floating eccentricity is also shown, along with the preferred circular orbit model.

(A color version of this figure is available in the online journal.)
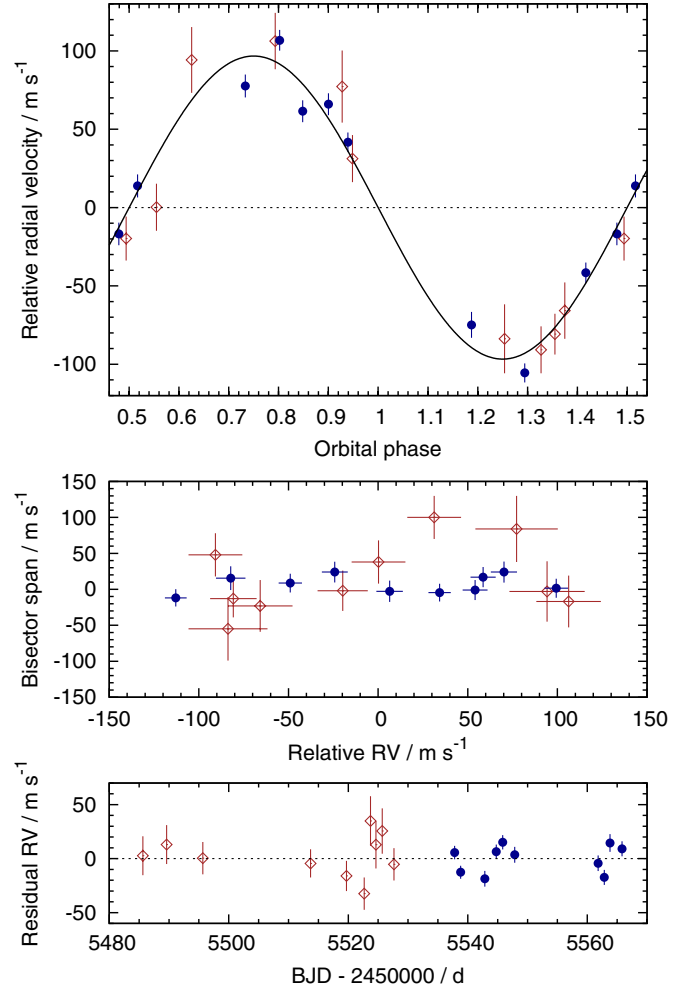

Figure 6. Radial velocity measurements for HAT-P-30/WASP-51: red diamonds and blue circles denote OHP and CORALIE observations, respectively. Details are as for WASP-35, with center-of-mass velocity, $\gamma = 44.68$ km s^{-1} here.

(A color version of this figure is available in the online journal.)

Table 6
Stellar Parameters of WASP-35, WASP-48, and HAT-P-30/WASP-51 from Spectroscopic Analysis

Parameter	WASP-35	WASP-48	HAT-P-30/WASP-51
$T_{\rm eff}$	6050 ± 100 K	6000 ± 150 K	6250 ± 100 K
$\log g$	4.4 ± 0.1	4.5 ± 0.15	4.3 ± 0.1
$\xi_{\rm t}$	1.3 ± 0.1 km s^{-1}	1.3 ± 0.2 km s^{-1}	1.3 ± 0.1 km s^{-1}
$v \sin i$	3.9 ± 0.4 km s^{-1}	12.2 ± 0.7 km s^{-1}	3.6 ± 0.4 km s^{-1}
[Fe/H]	-0.15 ± 0.09	-0.12 ± 0.12	-0.08 ± 0.08
[Na/H]	-0.16 ± 0.11	-0.14 ± 0.07	-0.11 ± 0.05
[Mg/H]	-0.01 ± 0.11	-0.09 ± 0.07	-0.08 ± 0.08
[Al/H]	$\cdots$	0.02 ± 0.14	$\cdots$
[Si/H]	-0.06 ± 0.05	0.04 ± 0.08	-0.01 ± 0.09
[Ca/H]	-0.01 ± 0.12	-0.10 ± 0.11	0.05 ± 0.12
[Sc/H]	-0.02 ± 0.07	0.13 ± 0.09	0.01 ± 0.06
[Ti/H]	-0.03 ± 0.10	0.02 ± 0.13	-0.03 ± 0.08
[V/H]	-0.13 ± 0.06	-0.17 ± 0.16	-0.10 ± 0.09
[Cr/H]	-0.10 ± 0.09	0.09 ± 0.16	-0.01 ± 0.06
[Mn/H]	-0.29 ± 0.08	$\cdots$	-0.27 ± 0.11
[Co/H]	-0.22 ± 0.10	$\cdots$	$\cdots$
[Ni/H]	-0.16 ± 0.07	-0.18 ± 0.09	-0.10 ± 0.06
$\log A$(Li)	2.35 ± 0.08	<1.3	2.96 ± 0.08
Mass	1.10 ± 0.08	$1.09 \pm 0.08 \, M_\odot$	$1.20 \pm 0.09 \, M_\odot$
Radius	1.09 ± 0.14	$1.09 \pm 0.14 \, R_\odot$	$1.28 \pm 0.17 \, R_\odot$

Note. Mass and radius estimates using the Torres et al. (2010) calibration.

around 100:1. For WASP-48, the SOPHIE spectra were co-added to produce a spectrum with a typical S/N of around 80:1. For HAT-P-30/WASP-51, the CORALIE spectra were co-added to produce a single spectrum with an average S/N of around 150:1. The standard pipeline reduction products were used in the analysis.

The analysis was performed using the methods given in Gillon et al. (2009). The Hα line was used to determine the effective temperature, $T_{\rm eff}$, while the Na I D and Mg I b lines were used as surface gravity, $\log g$ diagnostics. The elemental abundances were determined from equivalent-width measurements of several clean and unblended lines. Atomic line data were mainly taken from the Kurucz & Bell (1995) compilation, but with updated van der Waals broadening coefficients for lines in Barklem et al. (2000) and $\log gf$ values from Gonzalez & Laws (2000), Gonzalez et al. (2001), and Santos et al. (2004). A value for microturbulence, $\xi_{\rm t}$, was determined from Fe I using the method of Magain (1984). The parameters obtained from the analyses are listed in Table 6. The quoted error estimates include those given by the uncertainties in $T_{\rm eff}$, $\log g$, and $\xi_{\rm t}$, as well as the scatter due to measurement and atomic data uncertainties.

WASP-51b has recently been announced as HAT-P-30b (Johnson et al. 2011). A discrepancy between their results and ours is the value of host star metallicity: we find a value of [Fe/H] = −0.08 ± 0.08, whereas Johnson et al. (2011) report [Fe/H] = 0.13 ± 0.08, from an analysis using Spectroscopy Made Easy (SME; Valenti & Piskunov 1996). The difference is partly due to a different solar metallicity value adopted in the spectral analysis, where we use log A(Fe) = 7.54 ± 0.03 from Biemont et al. (1991), which is 0.04 dex higher than the current Asplund et al. (2009) solar value of log A(Fe) = 7.50 ± 0.04. We continue to use the Biemont et al. (1991) value for consistency between analyses rather than adjusting to new values as they are announced. Additionally, we allow the microturbulence value to float and be fitted, finding a best-fit value of 1.3 km s^{-1}, in excellent agreement with the calibration in Bruntt et al. (2010), compared to the assumed value of 0.85 km s^{-1} adopted by Valenti & Fischer (2005) and used in Johnson et al. (2011). Using the lower value of microturbulence would increase our [Fe/H] abundance by 0.07. The slight differences in $T_{\rm eff}$ and log g values, where Johnson et al. (2011) find $T_{\rm eff}$ = 6300 ± 90 and log g = 4.36 ± 0.03, result in a difference of a further 0.03 dex. These three factors combine to reduce the discrepancy to only 0.07 dex, which is within the quoted uncertainties.

The projected stellar rotation velocity ($v \sin i$) was determined by fitting the profiles of several unblended Fe I lines. Values for macroturbulence, $v_{\rm mac}$, of 3.3 ± 0.3 km s^{-1}, 3.2 ± 0.3 km s^{-1}, and 4.0 ± 0.3 km s^{-1} were assumed for WASP-35, WASP-48, and HAT-P-30/WASP-51, respectively, based on the calibration by Bruntt et al. (2010), and instrumental FWHM of 0.13 ± 0.01 Å, 0.15 ± 0.01 Å, and 0.11 ± 0.01 Å, respectively, determined from the telluric lines around 6300 Å. Best-fitting values of $v \sin i$ = 3.9 ± 0.4 km s^{-1}, 12.2 ± 0.7 km s^{-1}, and 3.6 ± 0.4 km s^{-1}, respectively, were obtained. This value for $v \sin i$ for HAT-P-30b/WASP-51b agrees with the value of 3.1 ± 0.2 km s^{-1} found by Johnson et al. (2011) via their fitting of the Rossiter–McLaughlin effect for this system, while they found a lower value of 2.2 ± 0.5 km s^{-1} from spectral line fitting. An alternative determination of the macroturbulence based on the tabulation by Gray (2008), rather than the new calibration from Bruntt et al. (2010), results in $v_{\rm mac}$ = 5.1 ± 0.3 km s^{-1}, leading to $v \sin i$ = 1.8 ± 0.4 km s^{-1}, which agrees with the value found by Johnson et al. (2011).

The lithium abundance in WASP-35 implies an age of $\gtrsim$2 Gyr according to the calibration of Sestito & Randich (2005), while the measured $v \sin i$ gives a rotational period of $P_{\rm rot} \simeq$ 14 ± 2 days, assuming i = 90°, which yields gyrochronological age of ~$2.2^{+1.4}_{-0.9}$ Gyr using the relation of Barnes (2007). A lack of stellar activity is indicated by the absence of Ca II H+K emission in the spectra.

The non-detection of lithium in the WASP-48 spectrum suggests that the star is several gigayears old, and the lack of any Ca H+K emission is consistent with this. However, the stellar rotation rate of 4.5 ± 0.6 days from the $v \sin i$ measurement implies an age of only ~$0.2^{+0.2}_{-0.1}$ Gyr using the Barnes (2007) gyrochronological relation. This discrepancy is discussed further below.

The presence of strong lithium absorption in the HAT-P-30/WASP-51 spectrum suggests that the star is $\lesssim$1 Gyr old. The stellar rotation period of 18.0 ± 3.1 days found from the $v \sin i$ measurement results in an age of ~$5.6^{+7.2}_{-2.9}$ Gyr, although this can be regarded as an upper limit, since the stellar rotation rate may be higher due to the unknown value of stellar inclination (i).

3.2. System Parameters

We simultaneously analyzed all photometry and radial velocity data using a Markov Chain Monte Carlo (MCMC) analysis, as set out in Collier Cameron et al. (2007), modified to calculate the mass of the host star with a calibration on $T_{\rm eff}$, log ρ, and [Fe/H] as described in Enoch et al. (2010). The photometry provides the stellar density (assuming the eccentricity of the planetary orbit is known) while the effective temperature and metallicity of the star are obtained through spectral analysis given above.

We initially allowed the value of the eccentricity of each planetary orbit to float, which resulted in values of $e = 0.057^{+0.064}_{-0.032}$, $e = 0.058^{+0.058}_{-0.035}$, and $e = 0.040^{+0.044}_{-0.028}$ for WASP-35b, WASP-48b, and HAT-P-30b/WASP-51b, respectively. However, in each case the χ^2 values in fitting the radial velocity data are lower for a circular orbit than the eccentric solutions found here: the eccentric solutions produce radial velocity χ^2 values of 4.5, 15.4, and 10.6 for WASP-35, WASP-48, and HAT-P-30/WASP-51, respectively, for 12, 14, and 20 RV data points, while a circular orbit for each results in χ^2 values of 0.60, 8.6, and 1.8. With no strong evidence for eccentricity in the orbits, we then performed second analyses of all systems, fixing the eccentricities to zero.

The MCMC results for WASP-48b reveal a slightly evolved star with a large radius of 1.75 $R_\odot$ (discussed below). This radius is around 0.6 $R_\odot$ greater than expected for that of a star of the same mass on the main sequence. To explore this, we performed a further analysis, imposing a main-sequence constraint on WASP-48, such that a Gaussian prior is used on the stellar radius at each step in the analysis, centered on radius $R_* = M_*^{0.8}$, again allowing the eccentricity to float. This forced the stellar radius estimate down to 1.13 $R_\odot$, artificially inflating the eccentricity estimate to 0.38 ± 0.04 to compensate, since the stellar radius is calculated from the photometry, including a term $\frac{1+e \sin \omega}{\sqrt{1-e^2}}$: an eccentricity of 0.4 produces a stellar radius value 0.65 times that of the estimate with eccentricity at zero. However, there is no evidence for such a high eccentricity in the radial velocity curve (see Figure 5) and the χ^2 values are 33.3 and 8.6 for eccentric and circular orbits, respectively (where there are effectively four degrees of freedom: radial velocity semi-amplitude, K, center-of-mass velocity, γ, eccentricity, e, and argument of periastron, ω). Imposing the main-sequence constraint with the eccentricity held fixed at zero decreases the stellar radius to 1.31 ± 0.09 $R_\odot$ and decreases the impact parameter from 0.7 to 0.4 to compensate: such a reduction in impact parameter leads directly to a stellar radius estimate 0.70 times smaller. However, the much lower impact parameter estimate produces a model that does not match well the high-quality follow-up photometric data: compare the fit to ingress and egress in Figure 7, showing the lower impact parameter model, with that in Figure 2. Since neither analysis with main-sequence constraint imposed produces realistic models for the photometry and spectroscopy, the results from the analysis with no main-sequence constraint are clearly preferred.

We also tested the imposition of the main-sequence constraint on WASP-35 and HAT-P-30/WASP-51, producing negligible change in all parameters, well within the parameter uncertainties, which implies that the photometry is sufficient to constrain well the results.

The best-fit parameters for each system, with eccentricity fixed to zero and no main-sequence constraint imposed, are given in Table 7, where HJD values are in HJD_UTC—see

Table 7
System Parameters from Simultaneous MCMC Analysis of All Photometric and Spectroscopic Data

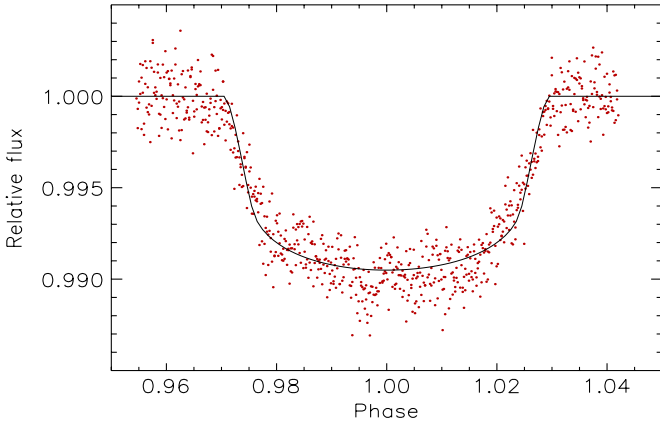| Parameter	Symbol	WASP-35	WASP-48	HAT-P-30/WASP-51
Period (days)	P	3.161575 ± 0.000002	2.143634 ± 0.000003	2.810603 ± 0.000008
Transit epoch (HJD)	T_0	5531.47907 ± 0.00015	5364.55043 ± 0.00042	5571.70057 ± 0.00016
Transit duration (days)	D	0.1278 ± 0.0009	0.1327 ± 0.0017	0.0920 ± 0.0008
Ingress/egress duration (days)	D_i	0.0154 ± 0.0004	0.0234 ± 0.0024	$0.0344^{+0.0027}_{-0.0018}$
Planet/star area ratio	R_p^2/R_*^2	0.0154 ± 0.0002	0.0096 ± 0.0002	0.0122 ± 0.0002
Impact parameter	b	$0.30^{+0.06}_{-0.09}$	0.73 ± 0.03	0.87 ± 0.01
Stellar reflex velocity (m s^{-1})	K_1	$94.82^{+7.11}_{-7.18}$	$136.02^{+11.04}_{-11.13}$	$96.70^{+6.19}_{-6.40}$
Centre-of-mass velocity (km s^{-1})	γ	17.718 ± 0.004	-19.683 ± 0.001	44.677 ± 0.001
Orbital separation (AU)	a	0.04317 ± 0.00033	0.03444 ± 0.00045	0.04118 ± 0.00031
Orbital inclination (deg)	i	$87.96^{+0.62}_{-0.49}$	$80.09^{+0.88}_{-0.79}$	$82.48^{+0.16}_{-0.15}$
Orbital eccentricity	e	0 (fixed)	0 (fixed)	0 (fixed)
Orbital distance/radius ratio	a/R_*	8.53 ± 0.19	$4.23^{+0.24}_{-0.19}$	6.67 ± 0.17
Stellar mass ($M_\odot$)	M_*	1.07 ± 0.03	1.19 ± 0.05	1.18 ± 0.03
Stellar radius ($R_\odot$)	R_*	1.09 ± 0.03	1.75 ± 0.09	1.33 ± 0.03
Stellar surface gravity (log $g_\odot$)	$\log g_*$	4.40 ± 0.02	4.03 ± 0.04	4.26 ± 0.01
Stellar density ($\rho_\odot$)	ρ_*	0.83 ± 0.07	0.22 ± 0.03	0.50 ± 0.02
Stellar metallicity	[Fe/H]	-0.15 ± 0.09	-0.12 ± 0.12	-0.08 ± 0.08
Stellar effective temperature	$T_{\rm eff}$	5990 ± 90	5920 ± 150	6250 ± 100
Planet mass (M_J)	M_p	0.72 ± 0.06	0.98 ± 0.09	0.76 ± 0.05
Planet radius (R_J)	R_p	1.32 ± 0.05	1.67 ± 0.10	1.42 ± 0.03
Planet surface gravity (log g_J)	$\log g_p$	2.98 ± 0.04	2.91 ± 0.06	2.93 ± 0.03
Planet density (ρ_J)	ρ_p	0.32 ± 0.04	0.21 ± 0.04	0.26 ± 0.03
Planet temperature ($A = 0, F = 1$) (K)	$T_{\rm eq}$	1450 ± 30	2030 ± 70	1710 ± 30

Figure 7. RISE photometry shown with the low impact parameter ($b = 0.4$) model; a poor fit compared to the fit with $b = 0.7$ in Figure 2.
(A color version of this figure is available in the online journal.)

Eastman et al. (2010) for conversion to alternative systems—and uncertainty values are from analyses where the follow-up photometry is binned to one-third of the ingress/egress duration (8, 10, and 14 minute bins for WASP-35, WASP-48, and WASP-51, respectively) to account for correlated noise (longer bins result in too few points in ingress/egress and hence large uncertainty in impact parameter). WASP-35 is found to have a mass of $1.07 \pm 0.03\, M_\odot$ and a radius of $1.09 \pm 0.03\, R_\odot$, while WASP-35b has a mass of $0.72 \pm 0.06\, M_J$ and a radius of $1.32 \pm 0.05\, R_J$, giving a density of $0.32 \pm 0.04\rho_J$. For WASP-48, the best-fit model gives a stellar mass of $1.19 \pm 0.05\, M_\odot$ and a radius of $1.75 \pm 0.09\, R_\odot$. WASP-48b is found to have a mass of $0.98 \pm 0.09\, M_J$ and a radius of $1.67 \pm 0.10\, R_J$, giving a density of $0.21 \pm 0.04\rho_J$.

The best-fit result for HAT-P-30/WASP-51 gave a stellar mass $1.18 \pm 0.03\, M_\odot$, stellar radius $1.33 \pm 0.03\, R_\odot$, planetary mass $0.76 \pm 0.05\, M_J$, and planetary radius $1.42 \pm 0.03\, R_J$,

giving a density of $0.26 \pm 0.03\rho_J$. Under the name HAT-P-30b, based on HAT-5 (Arizona) and HAT-9 (Hawaii) photometry of a total of around 3,200 good data points, follow-up high-quality photometric observations with Kepler-Cam on the FLWO 1.2 m telescope, and Keck and Subaru radial velocity measurements, Johnson et al. (2011) report a planetary mass of $0.71 \pm 0.03\, M_J$ and radius of $1.34 \pm 0.07\, R_J$, which agree with our values.

3.3. Isochrone Analysis

The values for stellar density, effective temperature, and metallicity from the MCMC analyses (MS constraint off, eccentricity fixed to zero) were used in an interpolation of the Padova stellar evolution tracks (Girardi et al. 2002; Marigo et al. 2008), shown in Figures 8–10. This resulted in an age for WASP-35 of 5.01 ± 1.16 Gyr and a mass of $1.03 \pm 0.04\, M_\odot$.

WASP-48 was found to have an age of $7.9^{+2.0}_{-1.6}$ Gyr and mass of $1.08 \pm 0.05\, M_\odot$, supporting the results from the MCMC analyses and lack of lithium and Ca H+K that WASP-48 is an old, slightly evolved star. However, the inferred age from the stellar rotation period is still only $0.6^{+0.4}_{-0.2}$ Gyr when based on a rotational period of 7.2 ± 0.5 days found from the larger stellar radius of $1.75 \pm 0.09\, R_\odot$ (with $v \sin i = 12.2 \pm 0.7$ km s^{-1}, as before). This apparent contradiction may be due to stellar spin-up by the planet. The close orbits of most known transiting exoplanets produce strong tidal forces between the planet and host star, which lead eventually to orbital circularization, synchronization, and decay. There is evidence for tidal circularization among the known transiting exoplanets, seen in the period–eccentricity relation where planets with very short orbital periods have circular orbits while those with longer periods show a range of eccentricities, but the synchronization of stellar rotation is generally ruled out for most known planet–star systems, with timescales of orders of magnitude larger than the Hubble time (Mazeh 2008; Pont 2009). A few exceptions exist where the companion is massive, e.g., the unique case of τ Boo for
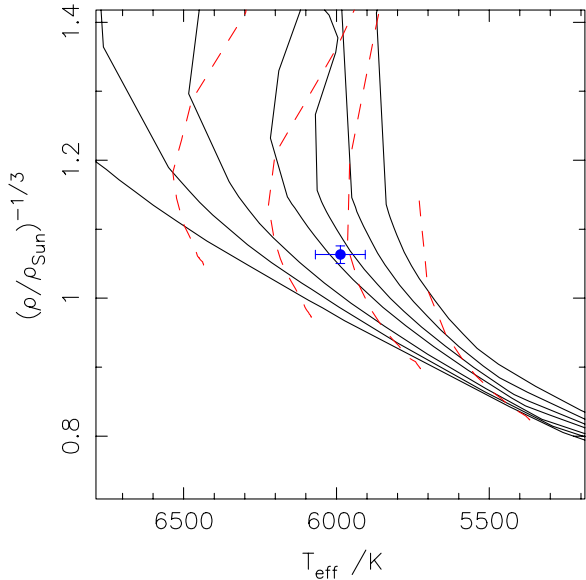
Figure 8. Isochrone tracks from Marigo et al. (2008) for WASP-35. Isochrones (solid lines, left to right) are 1.0, 1.99, 3.16, 5.01, 6.30, 7.94, and 10.0 Gyr. Evolutionary tracks (dashed lines) are for 1.2, 1.1, 1.0, and 0.9 $M_\odot$ stars.
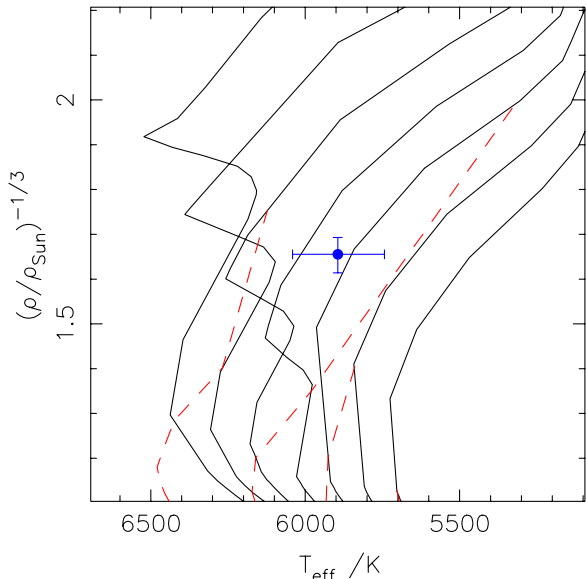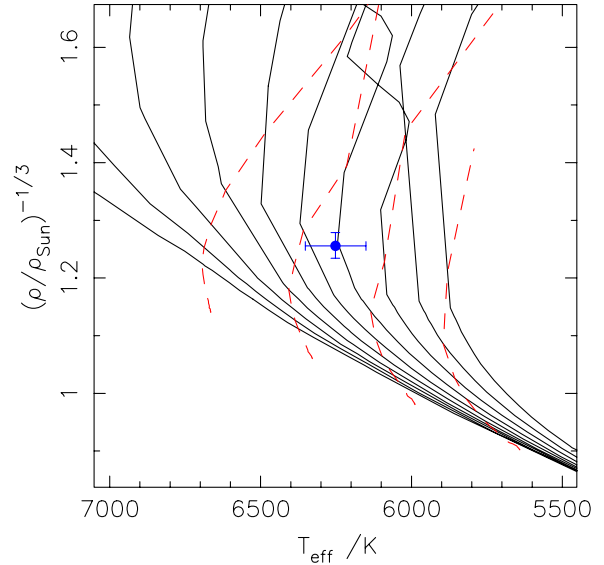(A color version of this figure is available in the online journal.)

Figure 10. Isochrone tracks from Marigo et al. (2008) for HAT-P-30/WASP-51. Isochrones (solid lines, left to right) are 1.0, 1.25, 1.58, 1.99, 2.51, 3.16, 3.98, 5.01, 6.30, and 7.94 Gyr. Evolutionary tracks (dashed lines) shown are for 1.3, 1.2, 1.1, and 1.0 $M_\odot$ stars.
(A color version of this figure is available in the online journal.)

An alternative analysis was also performed using the Yonsei-Yale isochrones (Demarque et al. 2004), which produced an age estimate of 4^{+2}_{-1} Gyr and a mass estimate of $1.04 \pm 0.04\ M_\odot$ for WASP-35, $6.0^{+2.0}_{-1.0}$ Gyr and $1.14^{+0.06}_{-0.07}\ M_\odot$ for WASP-48, and $3.0^{+1.0}_{-0.5}$ Gyr and $1.20^{+0.03}_{-0.05}\ M_\odot$ for HAT-P-30/WASP-51.

The results of both isochrone analyses are consistent within uncertainties, although the Padova interpolations yield higher ages for each system than the Yonsei-Yale interpolations, and mass values agree with the calibrated values from the MCMC analysis of $1.08 \pm 0.03\ M_\odot$, $1.19 \pm 0.05\ M_\odot$, and $1.18 \pm 0.03\ M_\odot$ for WASP-35, WASP-48, and HAT-P-30/WASP-51, respectively.

4. SUMMARY

We have presented observations of WASP-35b, WASP-48b, and HAT-P-30b/WASP-51b, new transiting exoplanets of 0.72 M_J and 1.32 R_J, 0.98 M_J and 1.67 R_J, and 0.76 M_J and 1.42 R_J, respectively. We have obtained photometry from both WASP-North and South instruments, as well as high-quality follow-up photometry from RISE, FTS, and TRAPPIST. Radial velocity measurements from the FIES, SOPHIE, and CORALIE instruments allowed us to confirm the planetary nature of the companions.

WASP-48b may have spun-up its slightly evolved host star, which shows a high $v \sin i$ value, otherwise contradicting the estimated stellar age of around 8 Gyr. HAT-P-30b/WASP-51b has recently been announced as HAT-P-30b, with mass 0.71 M_J and radius 1.34 R_J, values that agree with our results, within uncertainties.

Figure 9. Isochrone tracks from Marigo et al. (2008) for the slightly evolved WASP-48 (~8 Gyr, 1.75 $R_\odot$). Isochrones (solid lines, left to right) are 3.16, 3.98, 5.01, 6.30, 7.94, 10.0, and 12.5 Gyr. Evolutionary tracks (dashed lines) are for 1.2, 1.1, 1.0, and 0.9 $M_\odot$ stars.
(A color version of this figure is available in the online journal.)

which the planetary orbital period coincides closely with the mean rotation period of the stellar differential rotation pattern determined from the Zeeman–Doppler imaging (Fares et al. 2009). WASP-48b orbits with a period of 2.14 days ($a = 0.034$ AU), and while it is not a massive companion, the evolved nature of the star giving a radius of 1.75 $R_\odot$ results in a relatively short stellar tidal synchronization time of 11^{+3}_{-2} Gyr. A full tidal analysis will be discussed in the forthcoming paper of D. Brown (2011, in preparation).

For HAT-P-30/WASP-51, the interpolation yields an age of $4.0^{+1.0}_{-0.8}$ Gyr and mass of $1.16 \pm 0.04\ M_\odot$.

REFERENCES

Anderson, D. R., Hellier, C., Gillon, M., et al. 2010, ApJ, 709, 159
Anderson, D. R., Smith, A. M. S., Lanotte, A. A., et al. 2011, arXiv:1101.5620
Asplund, M., Grevesse, N., Sauval, A. J., & Scott, P. 2009, ARA&A, 47, 481
Baranne, A., Queloz, D., Mayor, M., et al. 1996, A&AS, 119, 373
Barklem, P. S., Piskunov, N., & O'Mara, B. J. 2000, A&AS, 142, 467
Barnes, S. A. 2007, ApJ, 669, 1167
Barros, S. C. C., Faedi, F., Collier Cameron, A., et al. 2011, A&A, 525, 54
Batygin, K., & Stevenson, D. J. 2010, ApJ, 714, L238
Batygin, K., Stevenson, D. J., & Bodenheimer, P. H. 2011, arXiv:1101.3800
Biemont, E., Baudoux, M., Kurucz, R. L., Ansbacher, W., & Pinnington, E. H. 1991, A&A, 249, 539
Bodenheimer, P., Laughlin, G., & Lin, D. N. C. 2003, ApJ, 592, 555
Bodenheimer, P., Lin, D. N. C., & Mardling, R. A. 2001, ApJ, 548, 466
Bouchy, F., Hébrard, G., Udry, S., et al. 2009, A&A, 505, 853
Bruntt, H., Bedding, T. R., Quirion, P. O., et al. 2010, MNRAS, 405, 1907
Burrows, A., Hubeny, I., Budaj, J., & Hubbard, W. B. 2007, ApJ, 661, 502
Charbonneau, D., Allen, L. E., Megeath, S. T., et al. 2005, ApJ, 626, 523
Charbonneau, D., Brown, T. M., Noyes, R. W., & Gilliland, R. L. 2002, ApJ, 568, 377
Collier Cameron, A., Wilson, D. M., West, R. G., et al. 2007, MNRAS, 380, 1230
Demarque, P., Woo, J., Kim, Y., & Yi, S. K. 2004, ApJS, 155, 667
Dhillon, V. S., Marsh, T. R., Stevenson, M. J., et al. 2007, MNRAS, 378, 825
Eastman, J., Siverd, R., & Gaudi, B. S. 2010, PASP, 122, 935
Enoch, B., Collier Cameron, A., Parley, N. R., & Hebb, L. 2010, A&A, 516, A33
Faedi, F., Barros, S. C. C., Anderson, D. R., et al. 2011, A&A, 531, 40
Fares, R., Donati, J., Moutou, C., et al. 2009, MNRAS, 398, 1383
Fortney, J. J., Marley, M. S., & Barnes, J. W. 2007, ApJ, 659, 1661
Gandolfi, D., Lanza, A. F., & Damiani, C. 2011, in Detection and Dynamics of Transiting Exoplanets, ed. F. Bouchy, R. Díaz, & C. Moutou (EPJ Web of Conferences, Vol. 11; Les Ulis: EDP Sciences), 05006
Gibson, N. P., Pollacco, D., Simpson, E. K., et al. 2008, A&A, 492, 603
Gillon, M., Smalley, B., Hebb, L., et al. 2009, A&A, 496, 259
Girardi, L., Bertelli, G., Bressan, A., et al. 2002, A&A, 391, 195
Gonzalez, G., & Laws, C. 2000, AJ, 119, 390
Gonzalez, G., Laws, C., Tyagi, S., & Reddy, B. E. 2001, AJ, 121, 432
Gray, D. F. (ed.) 2008, The Observation and Analysis of Stellar Photospheres (Cambridge: Cambridge Univ. Press)
Guillot, T., Burrows, A., Hubbard, W. B., Lunine, J. I., & Saumon, D. 1996, ApJ, 459, L35
Guillot, T., & Showman, A. P. 2002, A&A, 385, 156
Haswell, C. A. 2010, Transiting Exoplanets (Cambridge: Cambridge Univ. Press)
Høg, E., Fabricius, C., Makarov, V. V., et al. 2000, A&A, 355, L27
Jackson, B., Greenberg, R., & Barnes, R. 2008, ApJ, 681, 1631
Johnson, J. A., Winn, J. N., Hartman, J. D., et al. 2011, ApJ, 735, 24
Kurucz, R. L., & Bell, B. 1995, Atomic Line Data, Kurucz CD-ROM No. 23 (Cambridge, MA: Smithsonian Astrophysical Observatory), 23
Latham, D. W., Borucki, W. J., Koch, D. G., et al. 2010, ApJ, 713, L140
Magain, P. 1984, A&A, 134, 189
Mandushev, G., O'Donovan, F. T., Charbonneau, D., et al. 2007, ApJ, 667, L195
Marigo, P., Girardi, L., Bressan, A., et al. 2008, A&A, 482, 883
Mayor, M., Udry, S., Lovis, C., et al. 2009, A&A, 493, 639
Mazeh, T. 2008, in Tidal Effects in Stars, Planets, and Disks, ed. M.-J. Goupil & J.-P. Zahn (EAS Publications Series, Vol. 29; Les Ulis: EDP Sciences), 1
Perruchot, S., Kohler, D., Bouchy, F., et al. 2008, Proc. SPIE, 7014, 17
Pollacco, D., Skillen, I., Collier Cameron, A., et al. 2008, MNRAS, 385, 1576
Pollacco, D. L., Skillen, I., Cameron, A. C., et al. 2006, PASP, 118, 1407
Pont, F. 2009, MNRAS, 396, 1789
Queloz, D., Henry, G. W., Sivan, J. P., et al. 2001, A&A, 379, 279
Santos, N. C., Israelian, G., & Mayor, M. 2004, VizieR Online Data Catalog, 341, 51153
Seager, S., & Deming, D. 2010, ARA&A, 48, 631
Sestito, P., & Randich, S. 2005, A&A, 442, 615
Steele, I. A., Bates, S. D., Gibson, N., et al. 2008, Proc. SPIE, 7014, 217
Torres, G., Andersen, J., & Giménez, A. 2010, A&ARv, 18, 67
Triaud, A. H. M. J., Collier Cameron, A., Queloz, D., et al. 2010, A&A, 524, 25
Valenti, J. A., & Fischer, D. A. 2005, ApJS, 159, 141
Valenti, J. A., & Piskunov, N. 1996, A&AS, 118, 595